

## SUPPORTING INFORMATION

### Degradation of $(\text{La}_{0.6}\text{Sr}_{0.4})_{0.95}(\text{Co}_{0.2}\text{Fe}_{0.8})\text{O}_{3-\delta}$ Solid Oxide Fuel Cell Cathodes at the Nanometre Scale and Below

Na Ni<sup>1\*</sup>, Samuel J. Cooper<sup>1</sup>, Robert Williams<sup>2</sup>, Nils Kemen<sup>1</sup>, David W. McComb<sup>2</sup> and Stephen J. Skinner<sup>1</sup>

<sup>1</sup> Imperial College London, Exhibition road, SW7 2AZ London UK

<sup>2</sup> Center for Electron Microscopy and Analysis, Ohio State University, 1305 Kinnear Road, Columbus, OH 43212, USA

\*n.ni@imperial.ac.uk

## SUPPORTING INFORMATION

### 1. Electrode preparation

Ce<sub>0.9</sub>Gd<sub>0.1</sub>O<sub>2-x</sub> (CGO) pellets with dimensions of 10 mm in diameter and 2 mm in thickness were obtained from CGO powder (99.9%, Praxair, Danbury, Connecticut, USA) by uniaxially pressing at 2 MPa for 20s followed by isostatic pressing at 400 MPa for 30 s. The samples were sintered at 1400 °C for 5 h in air with a heating rate and a cooling rate of 5 °C min<sup>-1</sup>. A LSCF6428 ink (Fuel Cell Materials, Lewis Center, OH, USA) was screen-printed in symmetrical cell configuration on to both sides of the CGO electrolytes with the same size of the CGO pellet and sintered at 1100 °C for 2 h in air with heating rate and a cooling rate of 5 °C min<sup>-1</sup>. The thickness of the LSCF6428 electrode is ~ 20 μm, as shown in Figure S1.

### 2. Cr poisoning of LSCF cathodes of the symmetric cell.

Cr stock solution of 1.22 mol l<sup>-1</sup> was prepared by dissolving Cr(NO<sub>3</sub>)<sub>3</sub>·9H<sub>2</sub>O (99% purity, Sigma-Aldrich Co. LLC, Dorset, UK) in ethanol. The solution was dispensed into the electrode using a brush so as to fully wet the electrode in order to fill the pores and excess solution on the outer surface was removed using a swab. The impregnated sample was then heated at 900 °C for 5 hours to allow for any rapid reaction between Cr and LSCF. Reference samples without Cr impregnation were prepared and heat treated in the same condition and investigated as a reference. During the heat treatment, both reference and poisoned samples were imbedded in LSCF6428 powder with the same nominal composition (La<sub>0.60</sub>Sr<sub>0.40</sub>)<sub>0.95</sub>(Co<sub>0.20</sub>Fe<sub>0.80</sub>)O<sub>3-x</sub>, (Fuel Cell Materials, Lewis Center, OH, USA)

### 3. FIB-SEM tomography

The samples were first infiltrated with a commercial embedding resin (Epon\_812 substitute, MNA, DDSA and DMP, Sigma-Aldrich Co. LLC, Dorset, UK) in order to reduce the electrode porosity, which improves the SEM contrast so that the interference from the materials behind the current slice is minimized. A typical SEM micrograph of the individual slice is shown in Figure S2. The tortuosity factors of the electrode along the direction perpendicular to the electrode surface were estimated, based on the definition  $D_{\text{eff}} = D\varepsilon/\tau$ , from the reconstructed 3D volume using a finite-difference simulation developed in-house. This code, *TauFactor*, is packaged as a MatLab (MathWorks)

application and is freely available through the SourceForge distribution website<sup>2</sup>. To find the tortuosity factor of the solid phase, the Laplace equation was solved for the relevant phase, while the two boundaries of the control volume normal to the direction of interest were maintained at a fixed potential difference. These boundaries were imposed at the surface of the voxels using the ghost node principal and all other surfaces were considered to be insulating. The system of linear equations is then solved iteratively, employing vectorised and chequerboarded SOR (Successive Over-Relaxation) methods to speed convergence.

#### 4. Measurement of experimental k factors

To improve the EDX quantification in TEM, Experimental Cliff & Lorimer k factors<sup>3</sup> with respect to atomic ratio were obtained, with the definition of the k factors being:

$$\frac{C_A}{C_B} = k_{A,B} \cdot \frac{I_A}{I_B} \quad (1)$$

where  $C$  is the atomic concentration of element A or B, and  $I$  is the intensity of the chosen EDX lines of A or B. The sintered LSCF6428 electrode before any heat treatment was used as the standard and a stoichiometry of  $(\text{La}_{0.6}\text{Sr}_{0.4})_{0.95}(\text{Co}_{0.2}\text{Fe}_{0.8})\text{O}_3$  was assumed as the aim was to investigate the relative change of the composition between different samples.  $k_{\text{Cr,Sr}}$  was obtained by taking the  $\text{SrCrO}_x$  phase formed in the Cr poisoned sample as the standard and then the k factor of Cr-O was calculated by combining it with  $k_{\text{Sr,O}}$ . K lines were used for Sr, Co, Fe and O and the L Line was used for La. The background removal and deconvolution of overlapping of Cr-K and La-L lines was carried out using the “Tru-Q Analysis” algorithm implemented in Aztec software (Oxford Instruments, UK). Care has been taken when measuring EELS relative thicknesses to ensure that the quantification of other samples is carried out in areas having similar thickness as that of the area from which the k factor was determined (typically ~100 nm). K factors for EELS were obtained using a similar approach taking the sintered LSCF6428 electrode before any heat treatment as the standard. For EELS k factors, the analysis was carried out on spectra after the removal of multiple scattering with Fourier ratio deconvolution<sup>4</sup> to reduce the thickness effect. The obtained experimental k factors are listed in Table S2.

#### 5. Analysis of Fe valence

To analyze the B<sub>site</sub> valence, the common white-line ratio method<sup>5-7</sup> that relates the transition metal white line ratios ( $L_3/L_2$ ) with their valences was employed. The continuum background contribution to the L edges was subtracted by a double arctan function as developed by van Aken et al.<sup>8</sup>, which yielded a very small systematic error ( $\sim \pm 0.02-0.03$ ). After background subtraction, an integration window of 4 eV width centered at the  $L_2$  or  $L_3$  line was used to obtain the intensity of the white lines. As the specimen thickness is known to have a significant effect on the obtained ratio<sup>5</sup>, the effect of thickness was reduced by the removal of multiple scattering with Fourier ratio deconvolution<sup>4</sup>.

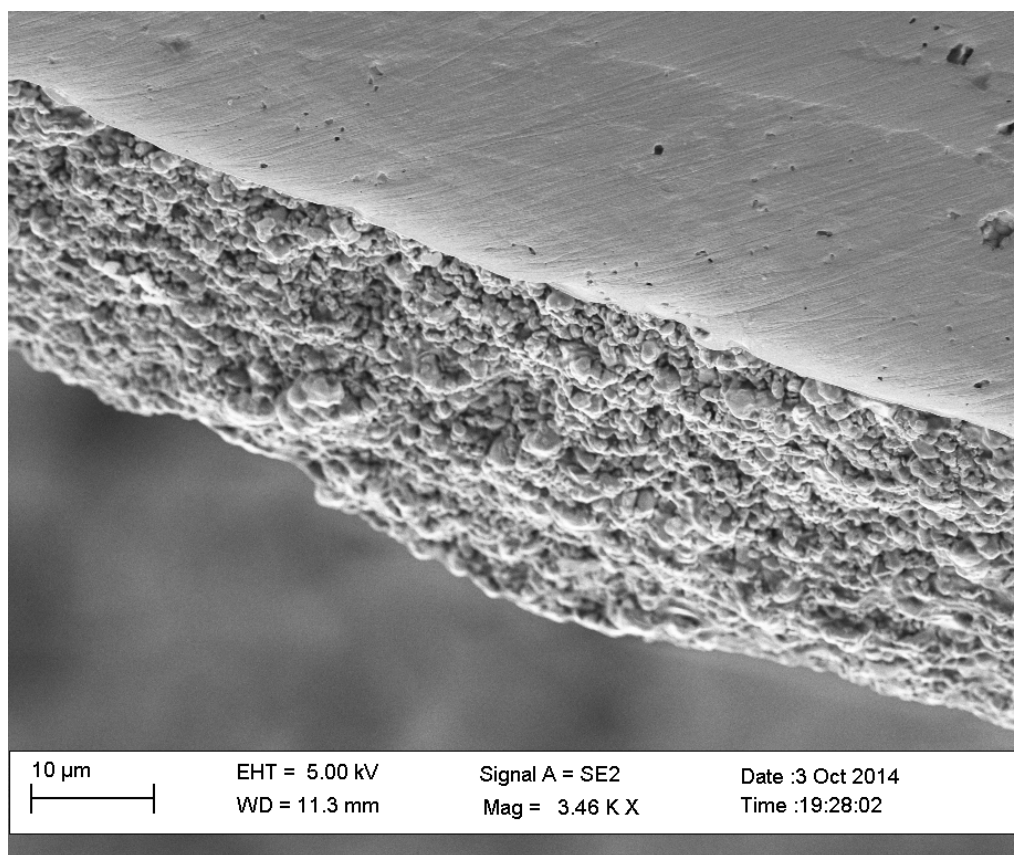


**Figure S1** Cross-sectional SEM micrograph of the LSCF6428 electrode on CGO.

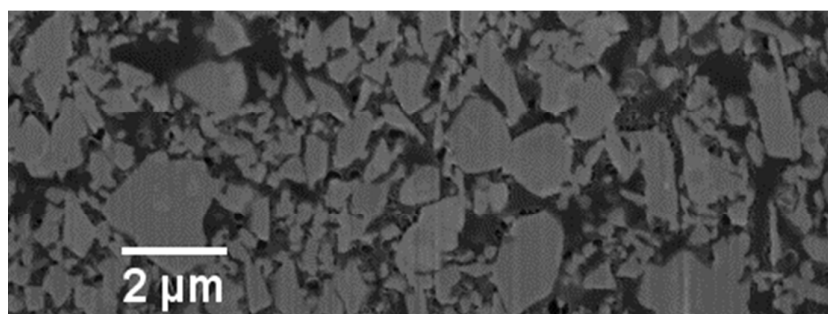


**Figure S2** SEM micrograph of an individual slice obtained with the FIB sectioning.

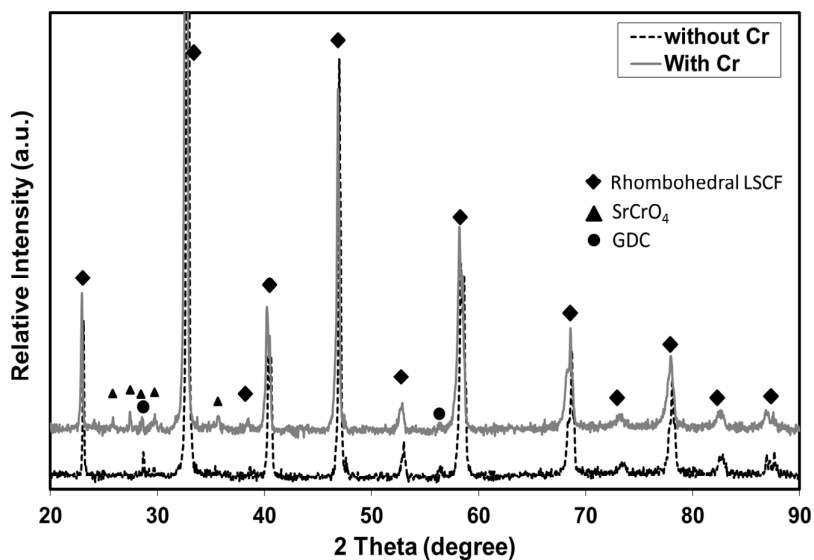


Figure S3 XRD characterization of the LSCF6428 cathode with and without Cr treatment.

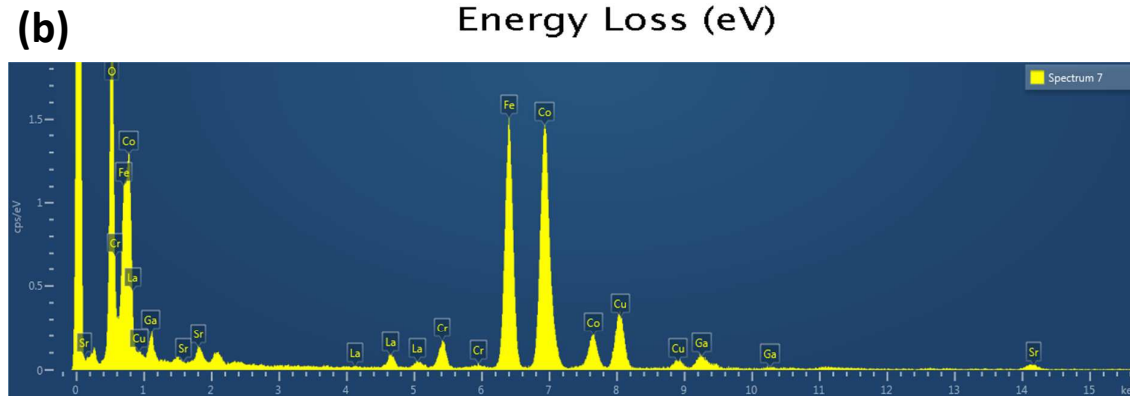
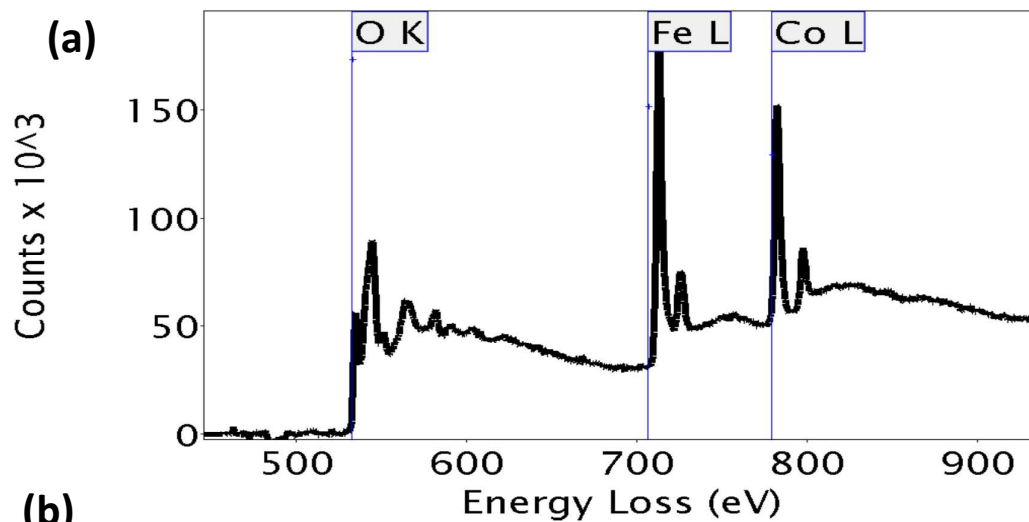
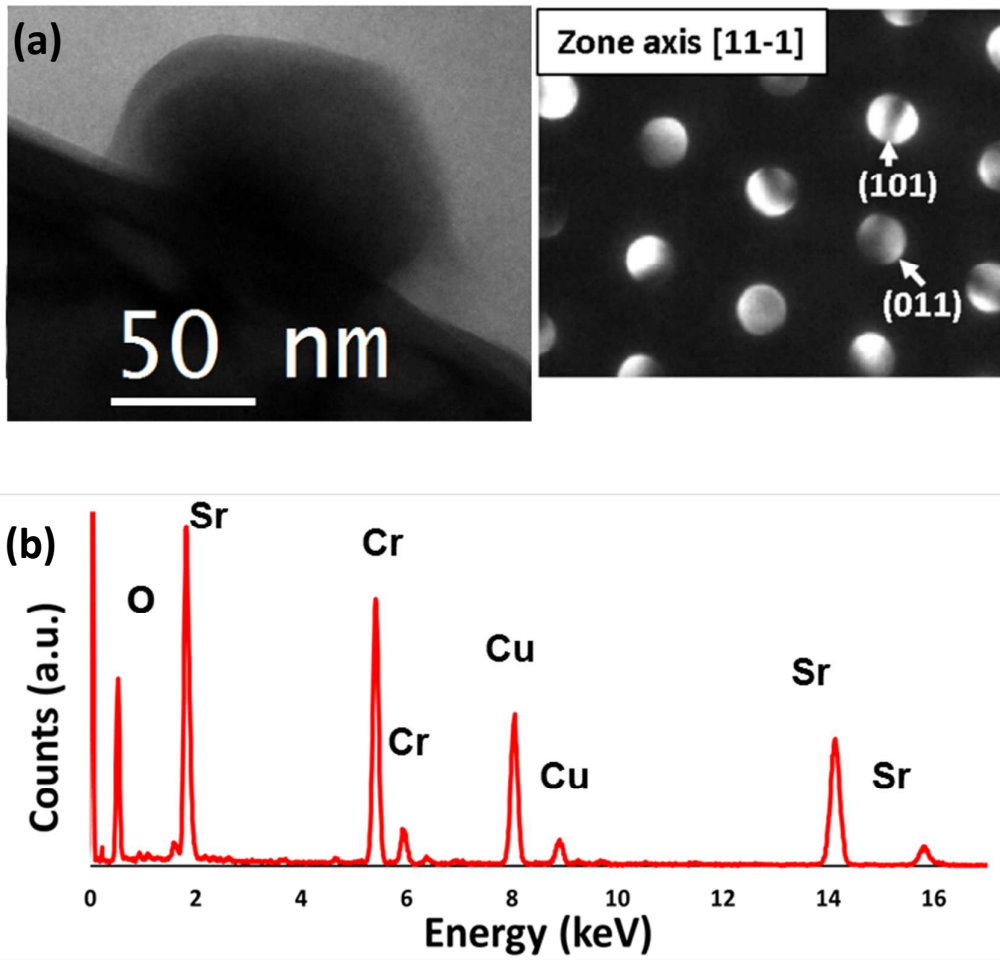
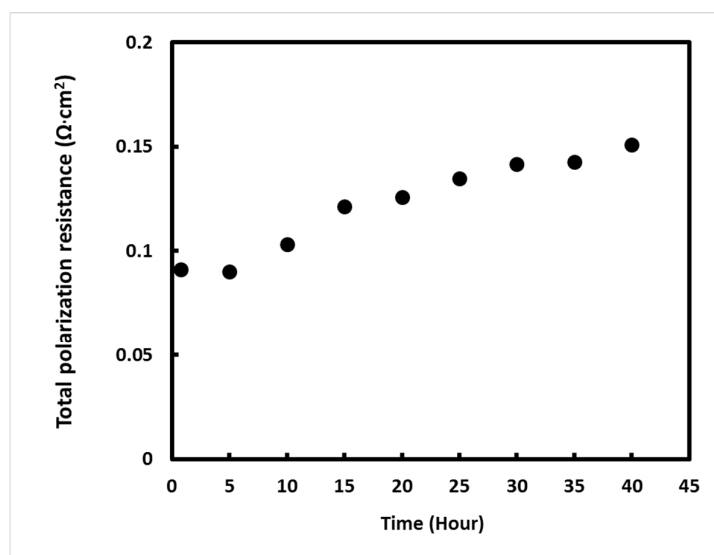


Figure S4 (a) EELS and (b) EDX spectrum from typical Fe-Co spinel particles as the one shown in Figure 4b. La, Cr and Sr signals are from adjacent grains as the spectrum was taken from an area to

increase the signal to noise ratio. Cu signal is from the TEM grid and Ga signal is an artefact resulting from the FIB process.



**Figure S5** (a) Bright field image of a typical  $\text{SrCrO}_4$  grain with indexed micro-diffraction pattern confirming the monoclinic structure. (b) STEM-EDX spectrum from the same grain.



**Figure S6** Change of the total polarization resistance (sum of the electrode resistance and the gas diffusion resistance) for the LSCF electrode as a function of heat treatment time at 900°C.

**Table S1** The fitted impedance parameters measured at 550 – 780 °C <sup>^</sup>

	Measure Temp (°C)	$R_0$ (Ω·cm <sup>2</sup> )	$R_1$ (Ω·cm <sup>2</sup> )	$C_1$ (F/cm <sup>2</sup> )	$R_2$ (Ω·cm <sup>2</sup> )	$C_2$ (F/cm <sup>2</sup> )	$R_{\text{electrode}}$ (Ω·cm <sup>2</sup> )
<b>Cr free reference sample</b>	780	4.16	0.0396	0.0127	0.0189	2.74	0.0396
	740	4.48	0.0920	0.00961	0.0187	2.57	0.0920
	690	5.01	0.224	0.00717	0.0123	6.45	0.224
	640	5.90	0.534	0.00591	0.0261	0.00428	0.566
	600	7.50	1.31	0.00512	0.258	0.00179	1.57
	550	10.6	3.48	0.00433	1.45	0.00154	4.93
<b>Cr poisoned sample</b>	780	8.21	0.377	0.0118	0.148	0.00457	0.525
	740	9.92	0.706	0.0138	0.434	0.00497	1.14
	690	11.7	1.91	0.0112	0.734	0.00437	2.64
	640	14.3	5.21	0.00971	1.81	0.00468	7.02
	600	20.8	18.0	0.00648	4.05	0.00435	22.1
	550	28.5	57.2	0.00616	16.8	0.00467	74.0

<sup>^</sup> The fitting error using the equivalent circuits during the analysis was typically between 1-5 %.

**Table S2 Experimental k factors for EDX and EELS**

	k <sub>La,O</sub>	k <sub>Sr,O</sub>	k <sub>Fe,O</sub>	k <sub>Co,O</sub>	k <sub>Sr,Cr</sub>	K <sub>Cr,O</sub>
<b>k (EDX)</b>	0.13±0.01	0.29±0.03	0.22±0.02	0.21±0.01	0.78±0.01	0.23±0.02
<b>k (EELS)</b>	0.30±0.01	/	0.53±0.02	1.05±0.10	/	/

## References

1. Cooper, S. J.; Eastwood, D. S.; Gelb, J.; Damblanc, G.; Brett, D. J. L.; Bradley, R. S.; Withers, P. J.; Lee, P. D.; Marquis, A. J.; Brandon, N. P.; Shearing, P. R. Image Based Modelling of Microstructural Heterogeneity in LiFePO<sub>4</sub> Electrodes for Li-ion Batteries. *J. Power Sources* **2014**, *247*, 1033-1039.
2. Cooper, S. J. Quantifying the Transport Properties of Solid Oxide Fuel Cell Electrodes. PhD Thesis, Department of Materials, Imperial College London, London, United Kingdom, **2016**.
3. Cliff, G.; Lorimer, G. W. The Quantitative Analysis of Thin Specimens. *J. Microsc. (Oxford, U. K.)* **1975**, *103* (2), 203-207.
4. Egerton, R. F. *Electron Energy-Loss Spectroscopy in the Electron Microscope*, 3rd ed.; Springer: New York, **2011**.
5. Tan, H.; Verbeeck, J.; Abakumov, A.; Van Tendeloo, G. Oxidation State and Chemical Shift Investigation in Transition Metal Oxides by EELS. *Ultramicroscopy* **2012**, *116*, 24-33.
6. van Aken, P. A.; Liebscher, B.; Styrsa, V. J. Quantitative Determination of Iron Oxidation States in Minerals using Fe L<sub>2,3</sub>-edge Electron Energy-Loss Near-Edge Structure Spectroscopy. *Phys. Chem. Miner.* **1998**, *25* (5), 323-327.
7. Garvie, L. A. J.; Buseck, P. R. Ratios of Ferrous to Ferric Iron From Nanometre-sized Areas in Minerals. *Nature* **1998**, *396* (6712), 667-670.
8. van Aken, P. A.; Liebscher, B. Quantification of Ferrous/ferric Ratios in Minerals: New Evaluation Schemes of Fe L<sub>23</sub> Electron Energy-Loss Near-Edge Spectra. *Phys. Chem. Miner.* **2002**, *29* (3), 188-200.